Laser Light Scattering Observations of Liquid–Liquid Phase Separation in a Polymer-Induced Liquid-Precursor (PILP) Mineralization Process

Elaine DiMasi* and Tianbo Liu[1]
Brookhaven National Laboratory, Upton NY 11973
Matthew J. Olszta[2] and Laurie B. Gower†
University of Florida, Gainesville FL 32611
[1]Present Address: Penn State University, State College PA 16802
[2]Present Address: Lehigh University, Bethlehem PA 18015
*Email address for correspondence: dimasi@bnl.gov
†Email address for correspondence: lgowe@mse.ufl.edu

ABSTRACT

A Polymer-Induced Liquid-Precursor (PILP) process for mineralization of calcium carbonate has been studied *in-situ* by laser light scattering. Static and dynamic light scattering data were obtained from $CaCl_2$ solutions containing poly(aspartic acid). Under these conditions calcium carbonate mineralizes through a liquid droplet precursor phase when the solution is exposed to the decomposition products of ammonium carbonate. Our measurements probe the integrated scatterer mass and the apparent hydrodynamic radius $R_{h,\mathrm{app}}$ of the droplets as they nucleate and coalesce. The data reveal three stages in the formation of the PILP phase: an early stage of droplet growth to $R_{h,\mathrm{app}} \approx 250$ nm; a mid-time stage of fluctuations and polydispersity in particle size; and a final growth period where $R_{h,\mathrm{app}}$ increases from 350 nm to the micron scale. Aggregation of precursor droplets, rather than atom-by-atom growth, is the dominant mechanism of mineral formation under these conditions. With respect to biomineralization, this first observation of 100-nm-scale droplets is significant, implying a possibility to mineralize from the liquid phase within the nanoscale compartments in which many biominerals form.

INTRODUCTION

The presence of biopolymers strongly affects mineralization from solution, through processes which are poorly understood but which are important in biomineralization and biomimetic materials science [1]. A number of different mechanisms have been described by which these macromolecules may affect the polytype or morphology of nucleating crystals, including stereochemical recognition [2, 3], charge redistribution at the organic interface [4], promotion of crystal nucleation [5], inhibition of a particular polytype [6, 7], and aggregation of proteins and crystallites [8]. The works cited above concern themselves with calcium carbonates, which are abundant as biogenic minerals and important to geochemistry. Much effort has been applied towards discerning relationships between the structural features of crystalline calcium carbonates and those of the organic matrices that control biomineralization.

A complete understanding of calcium carbonate biomineralization must include the amorphous, hydrated $CaCO_3$ phase. Amorphous phases and transitory precursors observed in biominerals have attracted recent interest [9, 10]. The amorphous phase is unstable relative to anhydrous $CaCO_3$ [11], converting to calcite under ambient laboratory

conditions, and under the combination of vacuum and irradiation in electron microscopes. Thus this phase may go unobserved in experiments, making it difficult to test theories depending on structural or stereochemical aspects of *crystalline* mineral phases which in fact may not be present at the time of nucleation. Batch crystallization of $CaCO_3$ in the presence of polymer additives has recently been observed *in-situ* by Raman Spectroscopy [6], but the authors concentrated on distinguishing between crystalline $CaCO_3$ polymorphs and did not address the possibility of amorphous precursors. More recent *in-situ* observations by x-ray reflectivity [12] and small-angle x-ray scattering [13, 14], have quantified the presence of *nanoscale* amorphous $CaCO_3$ films and particles during mineralization. This point is important to biomineralization, because biogenic minerals often form within compartments of submicron scale.

The formation of mineral-rich liquid phases, generated by the presence of acidic proteins or polypeptides, may underlie some biomineralization processes. Acidic polymers such as poly(acrylic acid) and poly(aspartic acid) are now known to drive calcium carbonate mineralization through a liquid-liquid phase separation process [15]. This Polymer-Induced Liquid-Precursor (PILP) process creates $CaCO_3$-rich droplets which can flow into confined spaces [16] and take the shape of surrounding boundary surfaces [17]. Upon dehydration, calcite crystals form which retain the fluidic shapes, yielding non-equilibrium morphologies which are evocative of biogenic calcium carbonate minerals. Up to now, observations of the liquid-liquid phase separation have been achieved only through optical microscopy, where PILP particles were observed to reach dimensions of 2–4 microns in diameter. Given the smoothness of the mineral films the PILP process can create, we suspected that much smaller droplets might be present initially, making the mineral-rich liquid phase a likely candidate for a precursor in biological mineralization processes, which often occur within nanoscale compartments.

The present paper confirms the submicron scale of mineral droplets created by the PILP process, using *in-situ* laser light scattering. Static light scattering measurements probe the integrated scatterer mass as a solution containing Ca-ion and poly(aspartate) is exposed to the decomposition products of ammonium carbonate salts, and precipitates hydrated $CaCO_3$ droplets. In the dynamic light scattering analysis, the fluctuations in the scattered light are converted to diffusion times related to an apparent hydrodynamic radius $R_{h,\mathrm{app}}$ that characterizes the scattering particles. Our data reveal three stages during formation of the PILP phase: an early stage of droplet growth to $R_{h,\mathrm{app}} \approx 250$ nm; a mid-time stage of fluctuations and polydispersity in particle size; and a final growth period where $R_{h,\mathrm{app}}$ increases from 350 nm to the micron scale.

EXPERIMENTAL DETAILS

Samples consisted of 10 ml volumes in light scattering cuvettes, containing 20 mM $CaCl_2$ plus 20 μg/ml Poly-(α, β)-D,L-Aspartic Acid, $M_w = 8600$ g/mol (from Sigma). Into the cap of the light scattering vial were placed crushed ammonium carbonate crystals, separated from the sample volume by a Handiwrap film. The solutions precipitated $CaCO_3$ within the closed volumes as the decomposition products of $(NH_4)_2CO_3$ (carbon dioxide and ammonia gases) diffused through the film. Light scattering measurements were made with a Brookhaven Instruments spectrometer operating at a wavelength of 532 nm. Static

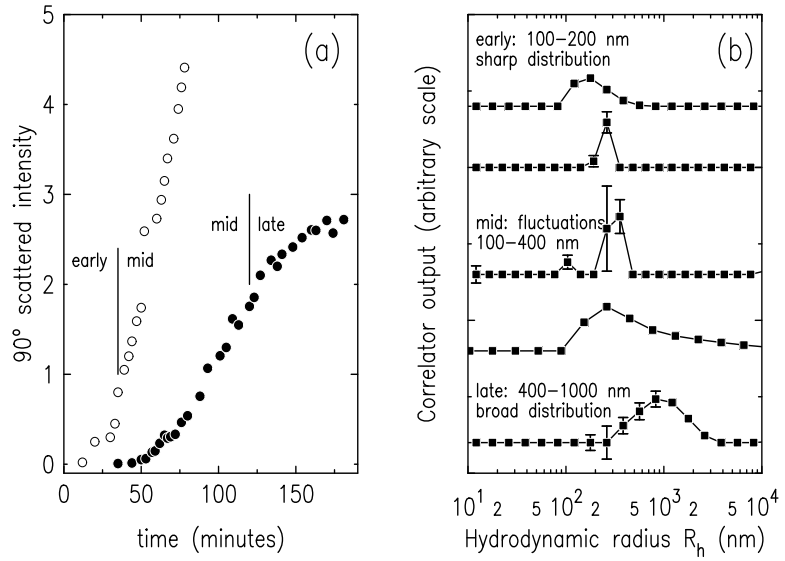

Figure 1: (a) Raw intensities for static light scattering data, at 90° scattering angle. Lines at the inflection points, separating early, mid and late times, are defined from the DLS data in Figure 2 (see text). Open and closed circles correspond to runs 1 and 3 of Figure 2. (b) Selected correlator output scans from runs 1 (early, mid) and 3 (late). Open and closed circles indicate scans from runs 1 and 3 respectively.

intensity was recorded at a 90° scattering angle with occasional spot checks at 60°. Dynamic light scattering data was obtained by CONTIN analysis of photon correlation measurements made at these angles. The dn/dc value for $CaCO_3$ is determined by calculation from the dn/dc values of $CaCl_2$, NH_4Cl and $(NH_4)_2CO_3$, which are measured by a commercial refractometer.

RESULTS

As droplets nucleate from solution within the sample cell, the measured static scattered light intensity increases monotonically (Figure 1(a)). Our interpretation of the scatterers as "droplets" rather than crystalline nuclei is supported by optical microscopy observations of additional reactions run under the same chemical conditions. Figure 3 is representative of the images taken, and shows the masses of droplets observable at the 10 μm scale after several hours, while only a few nascent calcite nuclei (which show color contrast under crossed polarizers) are present.

The static light scattering (SLS) signal can be attributed to small, interacting particles in the Rayleigh–Gans–Debye analysis:

$$Hc/R_0 = 1/M_w(1 + A_2c) \,,$$

where R_0 is determined from the experimental scattered intensity; H is a function of the optical properties including the dependence of the index of refraction upon solute mass concentration c; M_w is a weight average molecular weight characterizing the scattering particles; and the second virial coefficient A_2 contains information about particle

interactions. For the low solute concentrations used here, the measured intensity is proportional to the total scatterer masses in solution. Hence, the SLS experiment is a coarse measurement of the nucleation rate for the system. Because we were not able to control the gas diffusion rate in our experiments, the time dependences varied between different sample runs. Since the concentration of dissolved carbonate species (which affects the optical constant H) is increasing along with droplet concentration and/or individual masses of the droplets, SLS measurements are limited in their characterization of this system.

Further information is obtained from dynamic light scattering (DLS), which was also measured as a function of time during each reaction. In this measurement, the intensity–intensity time correlation function $G(\Gamma)$ is obtained by means of a digital correlator, yielding the distribution of apparent diffusion coefficients. The diffusion coefficient can then be related to an apparent hydrodynamic radius $R_{h,\mathrm{app}}$ by the Stokes-Einstein theory [18]. Representative particle size distributions are shown in Figure 1(b). The $R_{h,\mathrm{app}}$ distributions have different character in different time intervals. At early times, hydrodynamic radii are in the range 100–200 nm. Distributions are usually sharp, with intensity appearing in only one or two channels of the correlator (broad and narrow distributions observed are shown as examples). Midway into each experiment, the distribution of $R_{h,\mathrm{app}}$ exhibits slightly broader peaks, weaker intensities, and occasional bimodal distributions in particle size. Values of $R_{h,\mathrm{app}}$ measured during this mid-time regime have values between 100 and 450 nm. At late times, the hydrodynamic radius is observed to increase from about 300 to 800 nm, at which point the particles have reached the micron scale and are not well characterized by light scattering.

The $R_{h,\mathrm{app}}$ values we obtained for each data point in three different runs are compiled in Figure 2, where $R_{h,\mathrm{app}}$ is plotted against time. In Run 1, a roughly monotonic increase in $R_{h,\mathrm{app}}$ from 120 to 240 nm is observed for $t < 35$ minutes. After this, a bimodal $R_{h,\mathrm{app}}$ distribution appears (note the two $R_{h,\mathrm{app}}$ points for $t = 30$ min) and the $R_{h,\mathrm{app}}$ measurements fluctuate between 150 and 450 nm, showing that a wide range of particle sizes is present during this interval. Runs 2 and 3 do not exhibit an early period of growth, but start with a fluctuating $R_{h,\mathrm{app}}$ distribution in a similar range of $R_{h,\mathrm{app}} \leq 450$ nm. At late times in these experiments the particle size begins to increase, again monotonically, from 300 to 800 nm. Growth continues to the micron scale, but the scattering information is difficult to interpret properly at these large sizes.

DISCUSSION

Our observations of this Polymer-Induced Liquid-Precursor (PILP) process reveal three distinct stages in the nucleation and growth of amorphous mineral-precursor droplets. First we consider the early growth stage of Run 1. From $t = 17$ to $t = 32$ minutes, $R_{h,\mathrm{app}}$ increases from 112 to 258 nm, about a factor of two, while the normalized static scattered intensity also increases by about a factor of two. This suggests that the size increase is due principally to particle aggregation rather than continued precipitation from solution. If the particles were doubling in size due to more ions coming out of solution, each particle would increase its mass eightfold and this would have to be reflected in an eightfold increase in the total scatterer mass. Instead, the total mass has only doubled. Therefore, we surmise

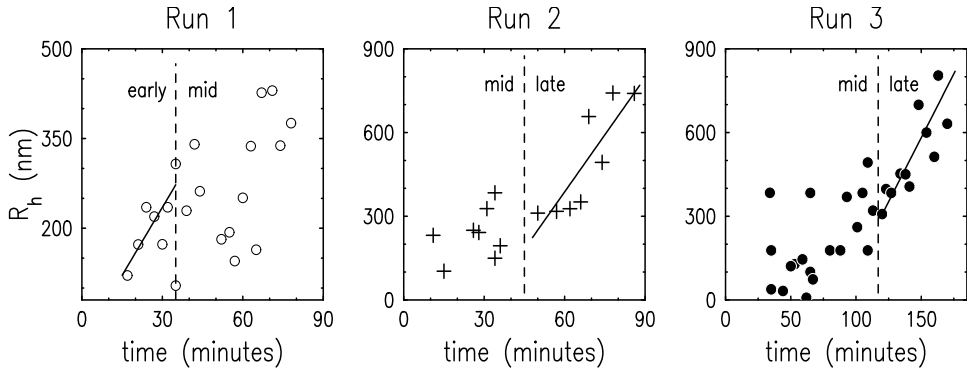

Figure 2: Apparent hydrodynamic radius $R_{h,\mathrm{app}}$ inferred from dynamic light scattering measurements vs. time for each of three separate experimental runs. Run 1 is characterized by an early stage of particle growth followed by a mid-time regime of large fluctuations and bimodal distributions in $R_{h,\mathrm{app}}$. Bimodal distributions in $R_{h,\mathrm{app}}$ are indicated by two separate data points at different $R_{h,\mathrm{app}}$ plotted at the same time point. Runs 2 and 3 began in the fluctuating $R_{h,\mathrm{app}}$ regime and finished with $R_{h,\mathrm{app}}$ growth from 300 to 800 nm. Lines in all panels are guides for the eye.

that particle aggregation is the predominant process during the times when particles are 100-250 nm in size.

In mid-time regions, the distribution of particle sizes is the same at the beginning and end of the interval. This generalization can be made for all three experimental runs shown in Figure 2 as well as for additional experiments we performed under varied conditions (data not shown). Although the particle size distribution was always the same for the duration of any mid-time interval we studied, the time dependence of the accompanying static data varied considerably. This interval therefore may reflect the continual addition of reactants to the solution, which occurs at variable rates. As long as the solution is supersaturated, the gas diffusion process provides a continuous source of the smallest particles, which aggregate as they encounter each other.

In the late stage of Run 3, $t = 120$–180 minutes, $R_{h,\mathrm{app}}$ increases from 300 to 800 nm (factor of 2.6), while the static intensity increases by a factor 1.5. Here we must note that at such large sizes the difference between $R_{h,\mathrm{app}}$ and the true particle size becomes significant, and one should be cautious in comparing $R_{h,\mathrm{app}}$ values directly. Nevertheless, the principal reason for the size increase must again be droplet aggregation. In our experiments we never observe increases of total scatterer mass that scale with $(R_{h,\mathrm{app}})^3$. Our optical microscopy experiments, conducted over a range of similar conditions, are compatible with this conclusion as many instances of micron-scale droplet aggregation have been observed, as suggested by the amassed droplets in Figure 3.

It is this observation, that 100-nm-scale droplets aggregate to form larger precursor particles under the control of dilute acidic polymer additives, which is most suggestive of a mechanism for biomineralization. Our past descriptions of micron-scale droplets formed by the PILP process (as observed by optical microscopy) were not sufficient to justify a mechanism able to deposit mineral precursor into submicron vesicular compartments, as

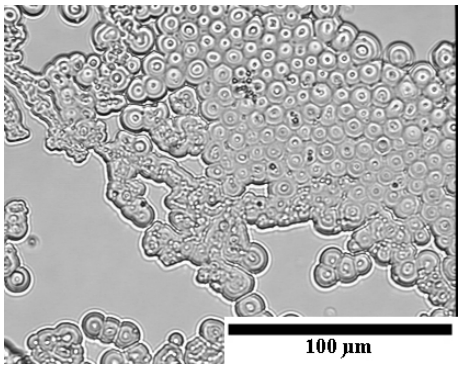

Figure 3: Optical micrograph (20x) of PILP droplets formed under conditions similar to those used for light scattering experiments. Droplets aggregate, but only partially coalesce, when reaching such a large size, presumably due to the partial dehydration and solidifcation that occurs by this late stage. Image acquired 4.5 hours after beginning exposure of the $CaCl_2$/Pasp solution to $(NH_4)_2CO_3$ salt vapors.

occurs during intracellular biomineralization. With the present measurements, we now know that submicron particles are nucleated by the polymer, and can be stable at small sizes on time scales much longer than those required for them to travel the relevant intercellular distances for biological mineral deposition. Thus it seems unlikely that the micron-scale droplets observed after several hours during our prior in-situ studies would be found in most biological systems. Instead, nanoscale droplets of precursor phase would gradually accumulate and coalesce with the forming biomineral.

Our solution-phase experiments prove that the acidic polymers induce phase separation even without a pre-existing calcite surface. Possibly the dissolved polymer acts as a nucleating substrate, as well as affecting the local crystallization kinetics by redistributing the ions in solution. In this context, it is interesting to compare recent observations by small-angle x-ray scattering (SAXS) of $CaCO_3$ nucleation from solution in the *absence* of polymer [13]. Here, rapid mixing of $CaCl_2$ and Na_2CO_3 produced a high supersaturation and the resulting colloidal $CaCO_3$ particles were observed by time-resolved synchrotron measurements, one objective being to identify transient metastable $CaCO_3$ species. The SAXS study observes particles which achieve sizes of 133 nm in 100 seconds. In subsequent studies, combined small- and wide-angle scattering demonstrated that the amorphous particles re-dissolve prior to the formation of calcite particles [14]. By contrast the presence of polymer in our light scattering study substantially inhibits particle growth, although it also enables larger clusters to form. Particle densities estimated by SAXS were found to be about half that expected for anhydrous $CaCO_3$ species and this was attributed to a hydrated, amorphous precursor phase [13, 14]. An almost identical observation has been made by our group for polymer-induced $CaCO_3$ precursor films nucleated at fatty acid monolayers at the water surface and studied by *in-situ* synchrotron x-ray reflectivity [12]. In the case of the surface films, increased proportions of polymer can lengthen the life of the precursor film, but do not strongly affect the kinetics of its growth or the subsequent transformation to calcite [DiMasi *et al*, manuscripts in preparation].

Combining the available observations from experiments with and without polymer additives, it appears that the hydrated precursor might be ubiquitous as a stage in $CaCO_3$ mineralization, but that an acidic polypeptide may be necessary to stabilize this precursor phase long enough for its fluidic morphology to be incorporated into the shape of the final crystalline product. It is this role that we believe is the most relevant to biomineralization processes, where proteins direct the minerals to form the specific complex morphologies that are incorporated into the well-known hierarchical structures. Illuminating the mechanisms by which organic species direct mineralization is the objective of our future studies on polymer-induced mineral precursor phases.

ACKNOWLEDGMENTS

This material is based upon work supported by the National Science Foundation under Grant No. DMR-0094209. We acknowledge additional support from the Particle Engineering Research Center (PERC) at the University of Florida, the Industrial Partners of PERC, NSF Grant EEC-94-02989, and NIH Grant RO1 DK59765-01. Brookhaven National Laboratory is supported under USDOE Contract DE-AC02-98CH10886.

REFERENCES

1. N. Dan, *TIBTECH* **18** (2000).
2. P. J. J. A. Buijnsters *et al*, *Langmuir* **17**, 3623 (2001).
3. Y.-J. Han and J. Aizenberg, *Angew. Chemie* **42**, 3668 (2003).
4. M. J. Lochhead, S. R. Letellier, and V. Vogel, *J. Phys. Chem. B* **101**, 10821 (1997).
5. L. Pach, Z. Hrabe, S. Komarneni, and R. Roy, *J. Mater. Res.* **5**, 2928 (1990).
6. P. Agarwal and K. A. Bergland, *Cryst. Growth Des.* **3**, 941 (2003).
7. I. W. Kim, R. E. Robertson, and R. Zand, *Cryst. Growth Des.* **5**, 513 (2005).
8. R. Lakshminarayanan, R. M. Kini, and S. Valiyaveettil, *PNAS* **99** (2002).
9. E. Beniash *et al*, *Proc. R. Soc. Lond.* **B**, 461 (1997).
10. F. Wilt, *J. Struct. Biol.* **126**, 216 (1999).
11. R. Brooks *et al*, *Proc. Royal Soc. London* **243A**, 145 (1950).
12. E. DiMasi, V. M. Patel, M. Sivakumar, M. J. Olszta, Y. P. Yang, and L. B. Gower, *Langmuir* **18**, 8902 (2002).
13. J. Bolze, B. Peng, N. Dingenouts, P. Panine, T. Narayanan, and M. Ballauff, *Langmuir* **18**, 8364 (2002).
14. D. Pontoni *et al*, *J. Phys. Chem. B* **107**, 5123 (2003).
15. L. B. Gower and D. J. Odom, *J. Crystal Growth* **210**, 719 (2000).
16. M. J. Olszta, E. P. Douglas, and L. B. Gower, in *Materials Inspired by Biology*, MRS Proceedings Volume 774, page 127, Warrendale PA (2003).
17. Y. Kim and L. B. Gower, in *Materials Inspired by Biology*, MRS Proceedings Volume 774, page 141, Warrendale PA (2003).
18. T. Liu, R. Rulkens, G. Wegner, and B. Chu, *Macromolecules* **31**, 6119 (1998).